

Experimental and Numerical Study of Residual Stress in the WC-12Co HVOF Sprayed Coatings

M. Jalali Azizpour^{a,*}, S. Nourouzi^b, H. Salimijazi^c, D. Sajedipour^a,
H. Mohammadi majd^a, F. Saadi^a

^a Department of Mechanical Engineering, Ahwaz branch, Islamic Azad University, Ahwaz, Iran.

^b Department of Mechanical Engineering, Babol University of technology, Babol, Iran.

^c Department of Materials Engineering, Isfahan University of Technology, Isfahan, Iran.

ARTICLE INFO

Article history:

Received 6 Nov 2013

Accepted 10 Dec 2013

Available online 25 Dec. 2013

Keywords:

HVOF

Peening stress

FEM

WC-12Co

XRD

ABSTRACT

Thermally sprayed coatings are intrinsically associated with residual stresses in the deposits. These stresses are varied in nature and magnitude, and have a pronounced effect on the mechanical behavior of the system. In the current study, WC-12Co coatings were deposited using HVOF thermal spraying. The $\sin^2\psi$ method was used to evaluate the through thickness residual stress by means of XRD after mechanical layer removal process. A nonlinear explicit-implicit finite element model was developed to study the peening and thermal stress during the high velocity impact of WC-12Co particle and cooling the splat and coating layers. The average of through thickness residual stress using X-Ray diffraction and numerical model was -157.1 MPa and -133.4 MPa respectively. The results showed that the residual stress was compressive and had a good agreement with the experimental results in literature.

1. Introduction

HERMAL spray coatings are extensively used for the protection of components from abrasive, adhesive and erosive wear, and corrosion. High-velocity oxygen-fuel (HVOF) spraying has shown to be one of the best methods for depositing WC-Co powders because of the higher velocities and lower temperatures experienced by the powder particles than other deposition methods, which results in less decomposition of the WC during spraying [1].

For thermally sprayed processes, residual stresses limit the thickness of the coating achieved due to the loss of adhesion between the deposit and substrate. Residual stresses in thermal spray coatings could be of a tensile or

compressive nature. Compressive residual stresses in the coatings have a beneficial effect on the bonding and fatigue behavior of the system [1]-[3]. However in HVOF processes which use lower spray temperatures and higher impact velocity particles than plasma spraying, significant peening stresses are produced due to the kinetic energy of the impinging particles to the substrate or previously deposited layer, inducing compressive residual stresses. Therefore, the final residual stress state through the whole coating-substrate system is determined by superposition of stresses of different nature induced during the spray process [4, 5]. Pina et al. [6] made same evaluation on the residual stresses of a HVOF

Corresponding author:

E-mail address: mjalali@iauhvaz.ac.ir (Mahdi Jalali Azizpour).

Table 1. Thermal spray parameters.

Parameter	Value
Fuel rate	250 m l/min
Oxygen rate	830 l/min
Spray distance	320 ±30 mm
Spray angle	90

WC-12Co coating by “ $\sin^2\psi$ ” method and reported the tensile stresses. Stokes and Looney [7] reported the tensile and compressive residual stresses on the surface and at the coating-substrate interface respectively. Y.Y. Santana et al. [8] determined the residual stresses profile WC-12Co coatings in two thickness (200 and 350 μm) employing conventional hole drilling method and XRD and found that the residual stress curve is not uniform through the coating thickness. Jalali et al. found the non-uniform compressive residual stresses in the same WC-12Co coating by means of electro discharge hole drilling [9].

The generation of in situ residual stresses during the plasma spray process has been simulated previously using FE modeling techniques [10, 11]. These models simulated the thermal effects only and did not include the peening stresses due to the reasons mentioned above. Stokes et al. [7] determined the residual stresses in a WC-Co coating by the analytical method advanced by Clyne et al. [12] and reported the presence of tensile surface stresses. R. Ghelichi et al. [13] had an experimental and numerical study on the residual stress in cold spray coatings.

In previous studies the stress state through the thickness of WC-Co coatings has not been studied using X-ray diffraction. Moreover the peening stress is not considered in numerical simulations. In present study, through thickness residual stress was measured using X-ray diffraction after layer removal process. Morphological studies were conducted using scanning electron microscopy (SEM) to evaluate the powder and coating characteristics.

A nonlinear explicit finite element methodology was developed to study the peening stress during the high velocity impact. In the next stage, these stresses were introduced in a layer deposition model as pre-stresses using an implicit analysis to predict the accumulated final residual stress state.

Attention was focused on the prediction of peening stress for a WC-12Co HVOF sprayed coating on an AISI 1045 substrate.

2. Experimental

AISI 1045 steel substrate samples were industrially coated by WC-12Co (80-71-1 Pulver, GTV mbh) using HVOF gun (Metjet III, Metallization). The substrates were grit blasted with 16 μm mesh SiC particles followed by ultrasonic cleaning in acetone. The average size of WC-12Co particle size was $\phi 24.73\mu\text{m}$ considering normal distribution histogram of powder particles. The spray parameters are tabulated in Table 1. Low stress grinding followed by mechanical removal using diamond strip p400-p 800 and 3-7-micron diamond paste was used to achieve desired surface. The residual stresses on the surface of coatings were determined by X-ray diffraction using Cu-K α radiation. The residual stress analysis was performed with PAN analytical X'Pert stress software. Morphological studies were conducted using scanning electron microscopy (SEM) to evaluate the powder and coating characteristics.

In this work, the residual stresses were predicted using an explicit-implicit FE methodology. The impact of a WC-Co solid single particle just below its melting temperature was modeled to predict the peening stress in coating and substrate, using the commercially available finite element (FE) solver ABAQUS/explicit. A two-dimensional axisymmetric model of a $\phi 25\mu\text{m}$ diameter WC-Co particle impacting on an AISI 1045 substrate disc of 1mm radius with 1mm thickness was generated using ABAQUS version 6.10. A dynamic, explicit temperature-displacement coupled analysis was carried out to study the high strain-rate impact process using ABAQUS/Explicit. Peening stresses were introduced in a layer deposition model as pre-stresses using an implicit analysis to predict the accumulated residual stress.

3. Results and Discussion

A. XRD and Morphological characterization

Fig. 1 illustrates the morphology of agglomerated WC-12Co powder using scanning electron

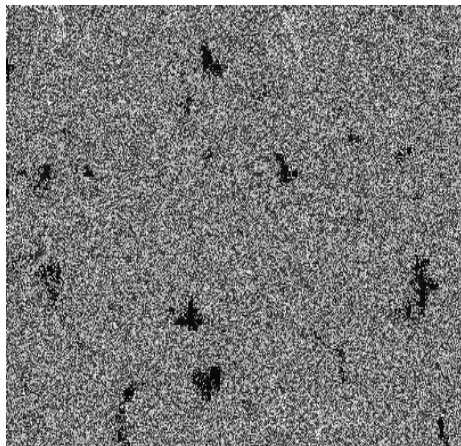


Fig. 1. SEM micrograph of WC-12Co powder particles

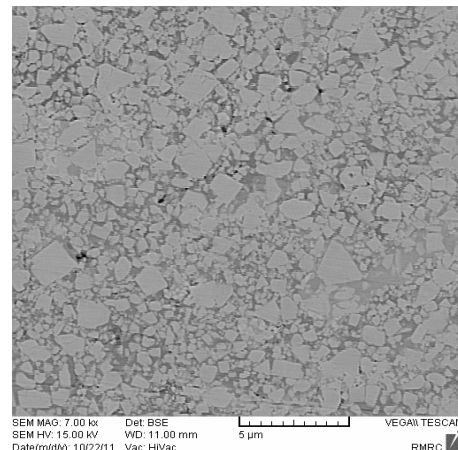


Fig. 2. SEM micrograph of WC-12Co coatings

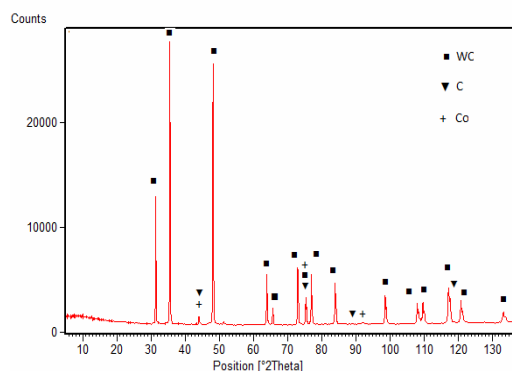


Fig. 3. XRD pattern of WC-12Co powder particles

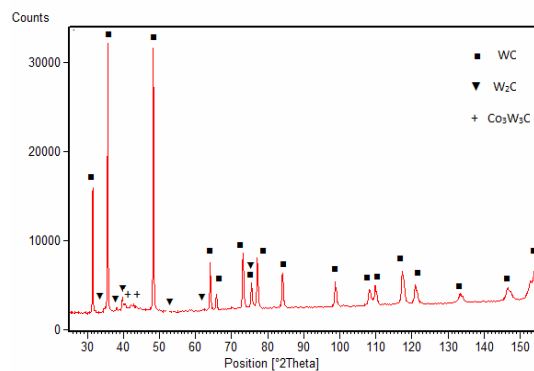


Fig. 4. XRD pattern of WC-12Co coating

microscopy. As observed the porous particles are spherical and have uniform size distribution. Fig. 2 illustrates a general view of the coating cross section after metallographic preparation. The WC-12Co HVOF thermally sprayed coating appears to be quiet dense.

XRD analysis was performed to evaluate the present phases in the WC-12Co powder and coating. Fig.3 illustrates the XRD pattern of WC-12Co powder. It can be seen from the patterns the peaks are attributed to WC and Co. The coating patterns (Fig.4) correspond to presence of WC, W₂C and Co₃W₃C in the coating. The average size of Nano-crystalline Co₃W₃C grains was calculated to be less than 9 nm using Scherer equation [14].The average size of Co₃W₃C matrix in this study was calculated to be 9.6µm.

B. Through thickness residual stress

X-ray diffraction technique is based on the fact that when a material is under stress the

resulting elastic strains make the atomic planes in polycrystalline structure to change their spacing. The position of the diffraction peak (2θ) undergoes shifting as the specimen is rotated by an angle psi (ψ). The shift of diffraction peaks is related to the magnitude of the residual stress [8]. For a residual stress measurement, the diffracting angle (θ), of interatomic planes of at least two different ψ angles have been measured. In absence of shear strains in the specimen, the ε and d spacing change linearly with sin²ψ. The relationship between measured strains and the residual stress (σ) is given [15]:

$$\epsilon_{\phi\psi} = \left[\frac{1+\nu}{E} (\sigma_1 \cos^2 \phi + \sigma_2 \sin^2 \phi) \sin^2 \psi \right] - \left[\frac{\nu}{E} (\sigma_1 + \sigma_2) \right] \quad [1]$$

As seen in Fig.5 the residual stress σ₁σ₂ plane can be described by:

$$\sigma_{\phi} = (\sigma_1 \cos^2 \phi) + (\sigma_2 \sin^2 \phi) \quad [2]$$

From Eq. 1 and Eq.2:

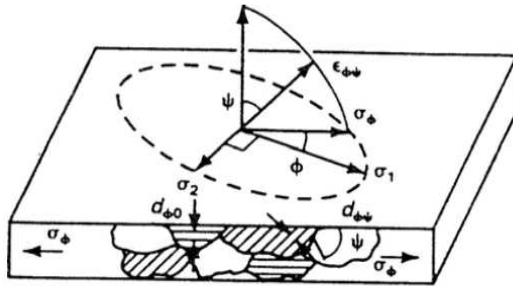


Fig. 5. Residual stress in free surface

$$\varepsilon_{\phi\psi} = \left[\frac{1+\nu}{E} \sigma_{\phi} \sin^2 \psi \right] - \left[\left(\frac{\nu}{E} \right) (\sigma_1 + \sigma_2) \right] \quad [3]$$

And for measured d-spacing versus residual stress:

$$d_{\phi\psi} = \left[\frac{1+\nu}{E} \sigma_{\phi} d_0 \sin^2 \psi \right] - \left[\left(\frac{\nu}{E} \right) d_0 (\sigma_1 + \sigma_2) - d_0 \right] \quad [4]$$

Where E is the Young's modulus, ν is Poisson's ratio, ψ is the tilt angle, $d_{\phi\psi}$ and $\varepsilon_{\phi\psi}$ are d-spacing and strain measured at each tilt angle.

For WC-12Co multiphase coating, the determined stresses by X-ray diffraction concern only the dominant phase(WC), which can be taken as the residual stresses on the surface of the coating [5, 16]. The strains in the samples were measured using peak position ($2\theta \sim 133.48^\circ$) of WC. Positive and negative tilts were applied over the full range for $\sin^2\psi=0$ up to 0.8 with step of 0.1.

The analysis results of the residual stresses in the WC phase on the surface of the as-coated and ground samples indicated a linear dependency of strains and d-spacing versus $\sin^2\psi$. Thus, it was assumed that the coating is under an equibiaxial stress state with $\sigma_{22}=\sigma_{33}$ and $\sigma_{11}=0$. Because the penetration depth of X-ray in WC-Co is very small ($\sim 2-5\mu\text{m}$) [15], [16] the resulting measurements refer specifically to surface of WC-Co coating thus only plane stresses were measured. As the measured strains for ($\psi<0$ and $\psi>0$) is linear function of $\sin^2\psi$, the shear stress components were negligible. So the residual stress can be obtained from the slop of strain- $\sin^2\psi$ plot:

$$\sigma_{\phi} = \frac{mE}{(1+\nu)} \quad [5]$$

The exact value of the elasticity modulus is

required for the evaluation of the residual stress. The elastic modulus test is based on the measurement of the elastic recovery of the Knoop indentation dimensions. The elasticity modulus of this coating was measured of 213 GPa using Knoop indentation as reported in previous published study [9].

As mentioned in literature [8] the grinding affected depth in WC-Co cermet is less than 1-2 mm so by using a proper mechanical removal process the effect of preparation method may be less than standard deviation of stress data [6]. The results of strain measurement in different layer after mechanical layer removal are illustrated in Figs.6-10. The through thickness residual stress was calculated from slop of strain- $\sin^2\psi$ plot and equation (3). Through thickness residual stress versus coating thickness is illustrated in Fig 11. The residual stresses are compressive except in layers just beneath the surface. The compressive residual stresses increase toward the interface. (The compressive residual stress is in its highest level near to coating-substrate interface). The Average of residual stress is -157.1 MPa

Residual stresses in WC-Co coatings have been evaluated experimentally by various researchers [6]-[8]. In our previous investigation the residual stress of -126 MPa was obtained in the same coating using electro-discharge hole drilling method as a non-contact drilling method [9]. The result of XRD method in this study has a good agreement with the result of residual stress measurement in WC-12Co coating using non-contact method. In Santana et al. research, experimental measurements of the residual stresses were made using XRD technique and the application-computed error of the measurements was of the order of 50MPa [8]. Measured stress in 350 μm thickness was found to be -180 MPa.

C. Through thickness residual stress

Impingement of sprayed particles can also be treated as a high-temperature shot-peening process. The impact of thermally sprayed particles onto a substrate is a non-linear dynamic contact event. The microscopic and macroscopic response of the impacting particle

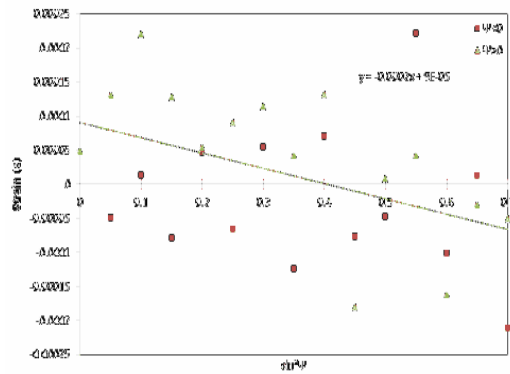


Fig. 6. Linear dependency of strain versus $\sin^2\psi$ in free surface

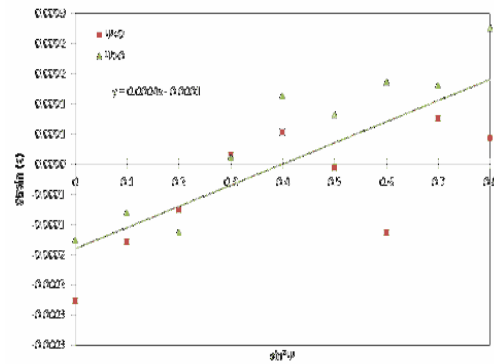


Fig. 7. Linear dependency of strain versus $\sin^2\psi$ in 50 μm thickness

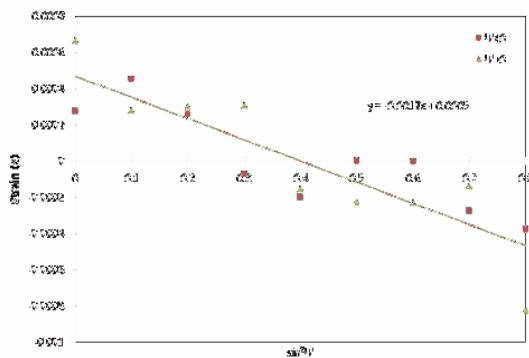


Fig. 8. Linear dependency of strain versus $\sin^2\psi$ 150 μm thickness

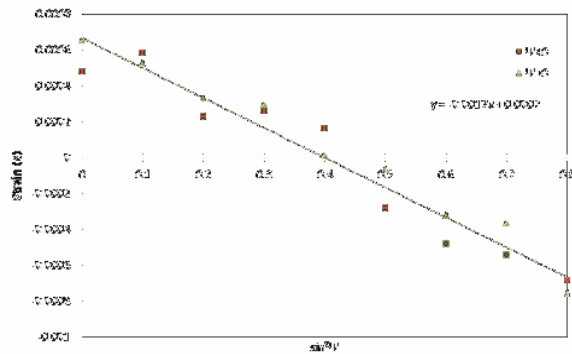


Fig. 9. Linear dependency of strain versus $\sin^2\psi$ 230 μm thickness

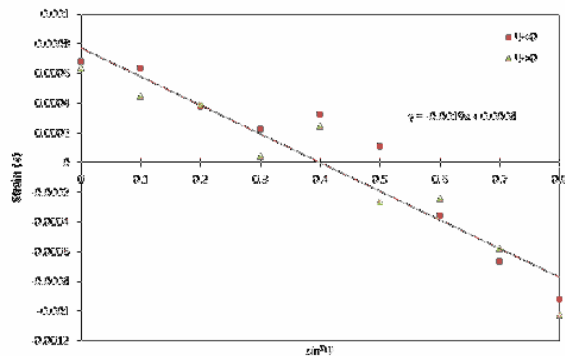


Fig. 10. Linear dependency of strain versus $\sin^2\psi$ 300 μm thickness

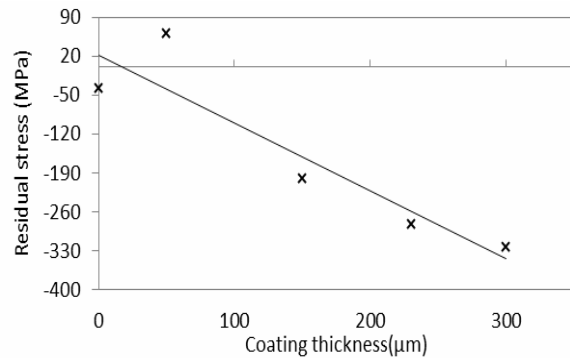


Fig. 11. Through thickness residual stress in WC-12Co Coating

and the underlying substrate under such loading conditions is strongly affected by the strain, strain rate, temperature and microstructure of the material. Using an appropriate constitutive equation defining the material properties are therefore essential for modeling such processes. The constitutive relation proposed by Johnson and Cook (the J-C model) is widely used in

numerical models involving high strain rates and temperatures and its use is generally limited to the impact of solids [17]. The J-C model is stated as follows:

$$\bar{\sigma} = \left[A + B(\bar{\epsilon}^{pl})^n \right] \left[1 + C \ln \left(\frac{\dot{\epsilon}^{pl}}{\dot{\epsilon}_0} \right) \right] (1 - \bar{T}^m) \quad [6]$$

Table 2. Parameters of J-C model [17], [18]

Model parameters J-C	WC-Co	AISI1045
A (MPa)	WC-Co	553.1
B(MPa)	1550	600.8
N	22000	0.234
C	0.45	0.013
M	0.016	1
Melting temp. K	1	1356
Reference strain rate (1/s)	1768	1

Table 3. Thermo physical properties of WC-Co [19]

Prameter	
Density(kg/mm ³)	14320
Solidus temperature(K)	1580
Liquidus temperature(K)	1640
Melting point (K)	1768
Specific heat(J/kgK)	295
Young's modulus(GPa)	331
Poisson's ratio	0.25
Latent heat(J/kg)	420,000

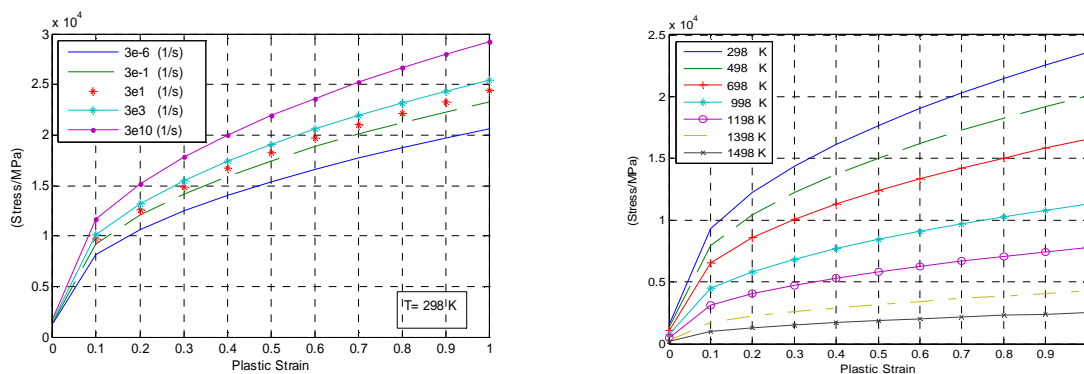


Fig. 12. Flow stress of WC-Co as a function of plastic strains for (a) different strain rates and (b) different temperatures ($\epsilon_0=1$)

$$\hat{T} = \frac{T - T_r}{T_m - T_r} \quad [7]$$

Where $\bar{\epsilon}^{pl}$ is the equivalent plastic strain, $\dot{\bar{\epsilon}}^{pl}$ is the equivalent plastic strain rate, and A, B, C, m and n are material parameters and $\dot{\epsilon}_0$ is the reference strain rate. \hat{T} is a non-dimensional temperature and T_r , T_m and T are room temperature, melting temperature and particle temperature respectively. J-C parameters and thermo-mechanical properties of AISI1045 substrate [18] and coating [19], [20] are given

in Table 2 and Table 3 respectively. Fig.12 and 13 illustrate the flow stress of WC-Co cermet and substrate respectively for different strains, temperatures and strain rates. It can be seen that the flow stress has higher values at higher strain rates and lower temperature. During the impact and plastic deformation of the particle, most of the kinetic energy of the particle will be transformed into heat (Eq.8).

$$T = T_r + \frac{\beta}{\rho c_p} \int \bar{\sigma} d\bar{\epsilon}_p \quad [8]$$

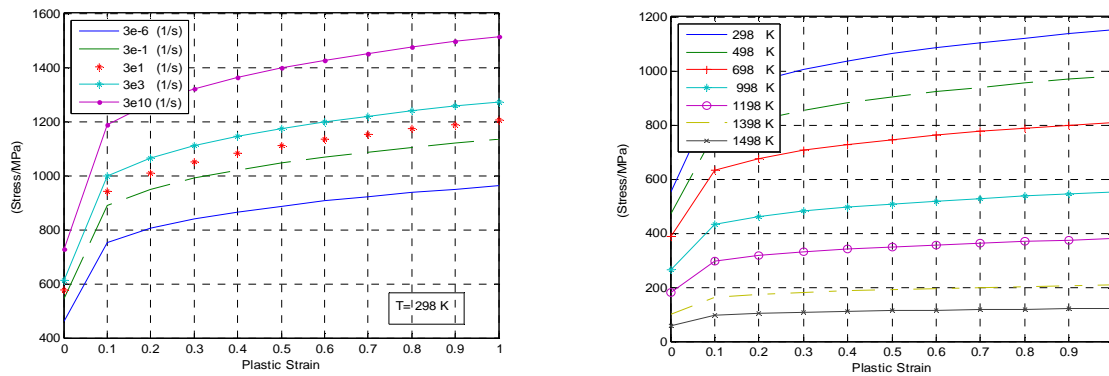


Fig. 13. Flow stress of AISI1045 as a function of plastic strains for (a) different strain rates and (b) different temperatures ($\epsilon_0=1$)

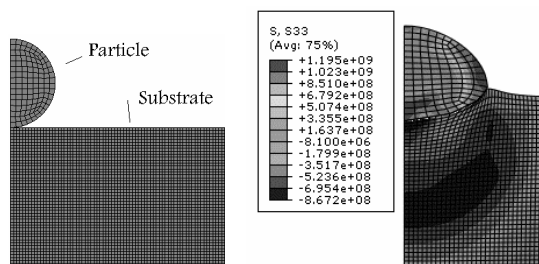


Fig. 14. 2-D model of (a) particle-substrate and (b) splat-substrate

Where β is the work to heat conversion factor, c_p is the heat capacity; ρ is the density. Hutchings [21] argued that, during impact of a particle with a metal target during an erosion process, more than 80% of the original kinetic energy of the particle was transformed into heat, with the rest of the energy being accounted for the stored energy of plastic deformation, the elastic wave energy and the rebound kinetic energy. In a more recent study of cold-spray deposition [22], it was assumed that 90% of the kinetic energy of the particle was dissipated into heat. Accordingly, in this work, it was assumed that 90% of the inelastic energy generated during impact was dissipated as heat.

D. Peening stress

A two-dimensional axisymmetric model of a $\phi 25 \mu\text{m}$ diameter WC-Co particle impacting on an AISI 1045 substrate disc of 1mm radius with 1 mm thickness was generated using ABAQUS version 6.10. A dynamic, explicit temperature-displacement coupled analysis was carried out to study the high strain-rate impact process

using ABAQUS/Explicit. In the model, spray conditions were characterized by the particle velocity and temperature. These parameters were considered as the key variables in the FE model and analyses were performed with the particle temperature of 1620 K and velocities of 350-450 m/s. The particles velocity is varied due to size distribution in sprayed powder. In this study it was assumed that the most of particles have a size near to the $\phi 25 \mu\text{m}$ and velocity of 375-450 m/s depends on the particle size. The WC-Co composite particle is considered as a single entity, with a single set of physical properties. In fact, the Co is heated, melted and then cooled and solidified, which binds the WC onto the substrate. However, temperatures in HVOF thermal spraying are not high enough to melt the WC phase.

Four-node linear displacement and temperature elements were used to discretize the particle and the substrate. All the displacements on the bottom face of the substrate were restrained. Symmetry boundary conditions were used on the left-hand side of the model. Upon impact, the sprayed particle deforms and spreads over the substrate, forming a splat. The FE analysis assumes that, after first contact, the particle remains attached to the substrate. This was implemented by assigning a no-separation criterion between the contacting nodes of the impinging particle and the underlying substrate. The contact was modeled using the kinematic contact method Fig.14 illustrates 2D axisymmetric model of the WC-Co particle and splat respectively on the substrate in $T=1620 \text{ K}$ and $V=425 \text{ m/s}$.

Fig. 15 illustrates the FE-predicted change on

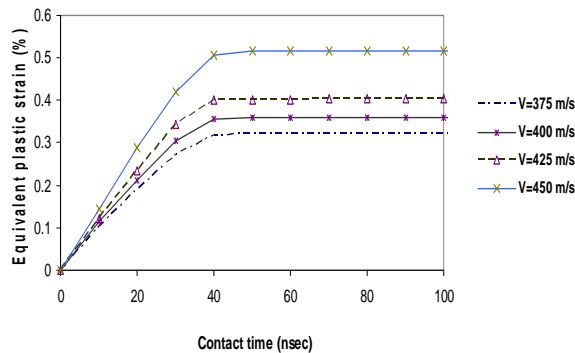


Fig. 15. FEM predicted plastic strain within 100 nsec after the impact in a selected node

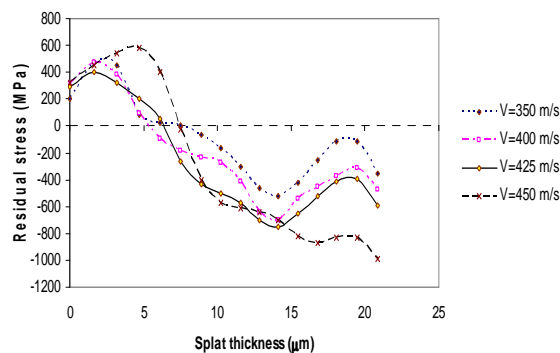


Fig. 17. FEM predicted peening stress (σ_{rr}) 100 nsec after the impact

the effective plastic strain in particle during impact. The particle starts to deform immediately after impact, causing the formation of a crater on the substrate. In the early stage of the impingement (50 ns), the deformation of the contact surface is evident. It clearly shows that after 50 ns there is no considerable change in plastic deformation and this is independent of particle velocity. However the plastic strains at higher velocities become greater in the same temperature contact. Fig. 16 shows residual stress versus impact time within 400 ns after initial impact. During the stress relaxation period within 100 ns after initial contact, the particle kinetic energy falls to zero. So in this model the impact time has chosen to be 100ns. Fig. 17 illustrates the stress distribution 100 ns after the initial contact where a WC-Co particle at temperature 1620 K is sprayed with impact velocities of 375-450 m/s toward an AISI1045 substrate. The direction is parallel to the free surface (radial direction). On the top of the particle the stresses are tensile. The stresses

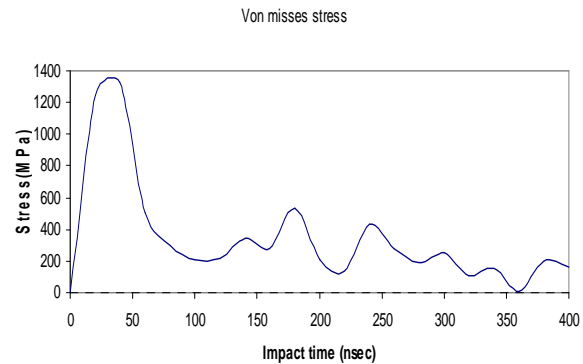


Fig. 16. FEM prediction of stress relaxation time during the impact

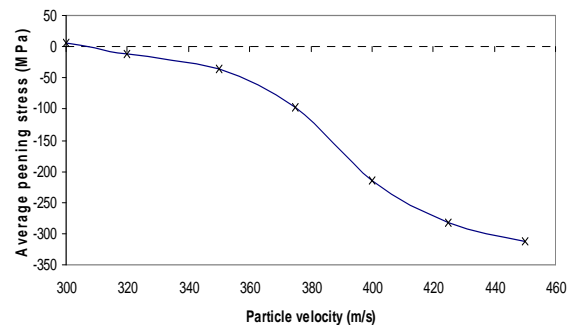


Fig. 18. FEM predicted peening stress profile (σ_{rr}) in various impact velocities

become compressive in few microns distance from the top of particle till the interface. Fig. 18 illustrates the predicted peening stress in splat at various impact velocities. The peening stress increases dramatically at impact velocities higher than sound velocity. In conventional plasma spraying which the particles do not have enough velocity and the temperature is relatively high, there are not considerable peening stresses. But in HVOF thermal spraying the velocities are more than sound velocity so the particles have enough kinetic energy to generate peening stress in coatings and substrate. For particles accelerated at $V=425$ m/s the average of peening stress were estimated to be -312 MPa. Fig. 19 illustrates the predicted peening stress field in the substrate in velocity of $V=425$ m/s after 100 nsec from the particle impingement. Upon impact, strong compressive stresses are predicted in the substrate up to a depth of 40 μ . Modeling of impingement process predicts that the highest compressive stresses are generated

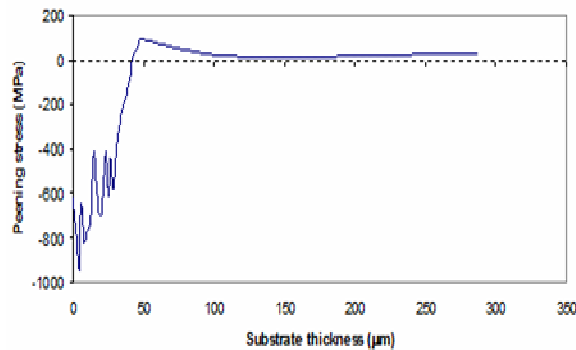


Fig. 19. FEM predicted peening stress profile (σ_{rr}) in substrate

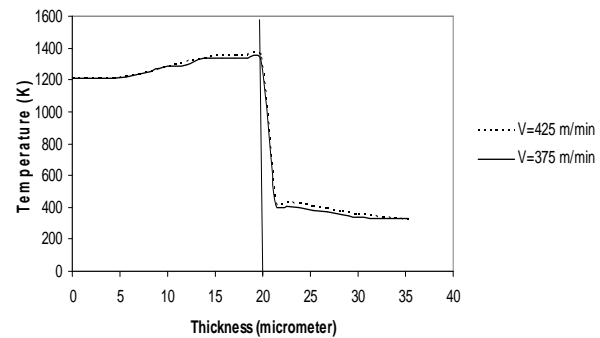


Fig. 20. FE-predicted temperature distribution across the splat and the substrate thickness after the impact ($T=1260$ K).

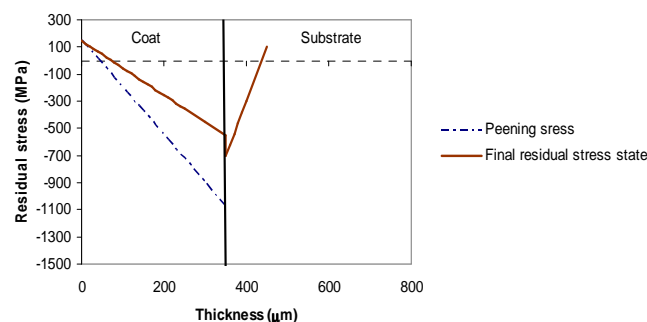


Fig. 21. FEM predicted of through thickness residual stress in coating and substrate

beneath the substrate surface on the center line of the particle.

Fig. 20 describes the predicted temperature distribution across the splat and the substrate thickness 100 ns after initial contact. An increase of approximately 130 K is predicted in the particle upon impact in 375m/s. The impact process also imposes extra heat to the substrate, and is predicted to affect a region up to about 40 μm deep. A greater temperature rise is predicted in the substrate along the particle–substrate interface when particles are sprayed at a velocity of 425 m/s. In this region, the temperature rises to 1345 K at 100 ns.

E. Final residual stress

In explicit analysis it is not possible to model the deposition of all layers on a particle – by – particle basis. Consequently, the present work develops a layer- by-layer deposition model by assuming that the average residual stress in a particle applies across the full width of the coating. In this study, ABAQUS standard linear solution, with 4-node thermally coupled axisymmetric elements was used. The elements

were displacement and temperature coupled with reduced integration and hourglass control.

Fig. 21 illustrates the residual stress distributions predicted by the finite element implicit layer analysis. This final stress state is the result of peening and thermal stresses generated during the HVOF thermal spraying process. The layer thickness in implicit model is 350 μm (~15 layers). The average of final residual stress was calculated to be -133.4 MPa.

FE-predicted stresses in the coatings sprayed with the particle velocities of 400-450 m/s have good agreement with the residual stress measured by means of XRD in this study and previous investigation with same coatings [9] . A comparison between the result of this study (experimental and numerical) and others studies is tabulated in Table 4.

The current model underestimates the compressive residual stresses. This could be attributed to the thermal spike generated by plastic deformation of unattached particles. Other stress relaxation mechanisms such as creep, microcracking and splat interfacial sliding which are not considered in developed

Table 4. The residual stress (MPa) measured by XRD and hole drilling

XRD	FEM	EDM [9]	XRD [8]	Curvature [9]
-157.1	-133.4	-126	-180	-164

model could have pronounced effect on residual stress. The differences between experimental and numerical results may be due to these stress relaxation effects.

4. Conclusions

X-ray diffraction was used to measure the through thickness residual stress in WC-12Co coatings. An explicit-implicit methodology was developed for predicting the generation of residual stresses in HVOF sprayed coatings. The explicit FE method was employed for modeling individual particle impact and the implicit method was used for a layer deposition model which takes as input the pre-residual stress and temperature distributions from the particle impact model. The model predicted similar distributions of the measured residual stress to this study and those reported in the literature. The results also emphasize the effect of peening stresses in control of residual stress state of the WC-Co coatings.

Acknowledgment

The authors gratefully acknowledge the R&D section of Poodrafshan Company and XRD section of Indian Institute of Technology (IIT), India.

References

1. P. Bansal, P. H. Shipway, S. B. Leen, "Residual stresses in high-velocity oxy-fuel thermally sprayed coatings – Modelling the effect of particle velocity and temperature during the spraying process," *Acta Materialia*, 55(15) 2007, 5089.
2. A. Ibrahim, C. C. Berndt, "Fatigue and deformation of HVOF sprayed WC-Co coatings and hard chrome plating" *Materials Science and Engineering* 456 2007, 114.
3. M. Cabrera, H. Sataia, "Fatigue behavior of a SAE 1045 steel coated with Colmonoy 88 alloy deposited by HVOF thermal spray" *Surface & Coatings Technology*, 205 (4) 2010, 1119.
4. C. Lyphout, "Residual Stresses Distribution through Thick HVOF Sprayed Inconel 718 Coatings," *J. Thermal spray Tech.*, 17(5) 2008, 915.
5. M. Jalali Azizpour, S. norouzi, H. mohammadi majd, H. Talebi, A. Ghamari, "Application of HVOF Thermal Spraying in High Speed Gas Compressor Shafts", *International Conference of Material, Mechanics and Aerospace Engineering*, The Netherlands. 45 2010, 360.
6. J. Pina, A. Dias, J. L. Lebrun, "Study by X-ray diffraction and mechanical analysis of the residual stress generation during thermal spraying" *Material Science Engineering*, 347 2003, 21.
7. J. Stokes, L. Looney, "Residual stress in HVOF thermally sprayed thick deposits" *Surface and Coatings Technology* 177 2004, 18.
8. Y. Y. Santana, "Characterization and residual stresses of WC-Co thermally sprayed coatings" *Surface & Coatings Technology* 202 2008, 4560.
9. M. Jalali Azizpour, S. Norouzi, H. reza Salimijazi, R. Moharrami, "Evaluation of Residual stress in HVOF thermally sprayed coatings using electro discharge machining", *Iranian J. of surface science*, 15 2013, 45.
10. B. S. Yilbas, A. F. M. Arif, "HVOF coating and laser treatment: three-point bending tests," *Surface & Coatings Technology* 202 2007, 559.
11. M. Toparli, F. Sen, O. Culha, E. Celik, *Journal of Materials Processing Technology* 190 2007, 26.
12. Y. C. Tsui, T. W. Clyne, "An analytical model for prediction residual stresses in progressively deposited coatings, Part1:Planar geometry" *Thin Solid Films* 306 1997, 23.
13. R. Ghelichi, S. Baferifard, D. MacDonald "Experimental and Numerical study of Residual Study in Cold Spray" *Applied Surface Science*, 288 2014, 26.
14. H. L. de Villiers Lovelock, "Powder/Processing Structure Relationships in WC-Co Thermal Spray Coatings: A Review of the Published Literature", *Journal of Thermal Spray Technology*, Volume 7(3)357, 1998.
15. S. Thaiwathana, N. Jantaping, P. Limthongkul, "Residual stress measurement of low temperature plasma surface alloyed layer using X-ray diffraction techniques," *Journal of surface engineering*, 28 (5) 2012, 273.
16. J. K. N. Murthy, D. S. Rao, B. Venkataraman, "Effect of grinding on the erosion behavior of a WC-Co-Cr coating deposited by HVOF and

- detonation gun spray processes”, *Wear*, 249 2001, 592.
- 17.GR. Johnson, Cook WH. In: Proceedings of the 7th international symposium on ballistics. The Netherlands; 541 1983.
- 18.S. P. Jaspers, J. H. Dautzenberg, “Material behavior in conditions similar to metal cutting: flow stress in the primary shear zone” *Journal of Materials Processing Technology*, 122 2002, 322.
- 19.P. J. Hazell, C. J. Roberson, M. Moutinho, “The design of mosaic armour: the influence of tile-size on the ballistic performance,” *Materials and Design*, 29 (8) 1497.
- 20.S. Kamnis, S. Gu, “Study of In-Flight and Impact Dynamics of Nonspherical Particles from HVOF Guns” :LK *Journal of Thermal Spray Technology*, 19(1) 2010, 31.
- 21.Hutchings IM. *Wear*; 70 1981, 269.
- 22.H. Assadi, F. Gartner, T. Stoltenhoff, H. Kreye. “Bonding mechanism in cold gas spraying” *Acta Mater*; 51 2003, 4379.

